
# USGS Verification and Validation Report
# Lunar South Pole Digital Elevation Model

**for**
**Program-NNH08ZDA008C**
**Scientific and Exploration Potential of the Lunar Poles**

**April 12, 2013**

**Submitted to:**

**Dr. Ben J. Bussey, Principal Investigator**
**The Johns Hopkins University Applied Physics Laboratory**
**11100 Johns Hopkins Road Laurel, MD 20723-6099**

**NASA Ames Research Center**
**Attn: Gregory K. Schmidt**
**Mail Stop: 17-1**
**Moffett Field, CA 94035**
**Reference: Agreement No. NNA09DB96I**

**Submitted by:**
**Mark R. Rosiek**
**USGS Astrogeology Science Center**
**2255 N. Gemini Drive, Flagstaff AZ 86001**

## Table of Contents

## Introduction

This report describes a Digital Elevation Model (DEM) generated from Lunar Reconnaissance Orbiter Camera (LROC) Narrow Angle Cameras (NAC) stereo pairs over the lunar south pole and provides a comparison to the Lunar Orbiter Laser Altimeter (LOLA) 5-m DEM (Neumann, 2010.) The methodology used to generate this DEM was changed from our previous procedures of registering the LROC NAC images to LOLA track data (Tran and others, 2010; Rosiek and others; 2012, Rosiek and others, 2013.) For this project we added registration of the LROC NAC images to the LOLA DEM. This change was possible and needed because the LOLA 5-m DEM is dense enough to support registration to the DEM and the number of LOLA track points is so large that we were unable to download all the LOLA altimeter points for the area being mapped and be efficient in using them. We only downloaded the altimeter points for several small patches throughout the area covered by the images. The SOCET SET®* (de Venecia and others, 2005; Zhang and others, 2006) sensor model was updated to accommodate images that crossed the pole, and other software modifications were made to map images that were captured while the spacecraft was rotating.

The resulting LROC NAC DEM has a post spacing of 4 m and contains 66,555,500 grid cells that cover an area of about 1,065 sq. km. The image coverage used to produce this DEM is provided in Figure 1. A color hillshade representation is provided in Figure 13 with a comparison to the LOLA DEM provided in Figure 14. A slope map is provided in Figure 23 and a comparison to the LOLA DEM is provided in Figure 24. The LROC NAC DEM improves upon the LOLA DEM in that the LROC NAC DEM is smoother and has been edited for major blunders. Within the LROC NAC DEM there are still errors due to seams of 1 – 5 m between the stereomodels. This is probably caused by spacecraft motion that is un-modeled and we provide recommendations in the conclusion section on research that may minimize these seams. Also, in areas of the LROC NAC DEM where the images are in shadow or along the edges of DEM there might be erroneous data that we did not catch during the editing process. Most of the differences (56%) between the LROC NAC and LOLA 5-m Grid DEM are within the expected difference of 2 m. The remainder of the differences can be attributed to seams between stereomodels, errors in shadow masking of the LROC NAC DEM, and errors in the LOLA 5-m Grid DEM caused by offsets in the LOLA track data; this last reason probably accounts for most of the differences. Slope values above 30° are unusual and might be erroneous; within the LROC NAC DEM only 0.78% of the slopes are above 30° and within the LOLA DEM there are 4.57% of the slope values above 30°.

## Source Data

The images used in this work came from the LROC NAC that can provide high-resolution images (0.5 to 2.0 m pixel scale) of key targets. LROC was not designed as a stereo system, but can obtain stereo pairs through images acquired from two orbits (with at least one off-nadir slew). Off-nadir rolls interfere with the data collection of the other instruments, so during the nominal mission LROC slew opportunities are limited to three per day (Tran and others, 2010.) In the polar regions the images are binned to accommodate the lower light levels and this reduces the resolution. The images we used had resolution values from 1.0 to 1.3 m.

* SOCET SET is a registered trademark of BAE Systems. Mention of trade names or manufacturers does not imply U.S. Government endorsement of commercial products.

### LROC NAC images

The LROC NAC images were acquired in four groups from 2010: 21 SEP, 23 SEP, 4 OCT, and 11 OCT. In Figure 1, the four different LROC NAC image groups are shown. Shadowed areas were eliminated in Figure 1. Only about 35% of an average image was in sunlight (range was 19% - 50 %.) Table 1 provides the percentage of the image pixels that were in sunlight broken out by the date the images were acquired.

| Table 1 - Percent of illuminated image pixels | | | | |
|---|---|---|---|---|
| Date | Avg % | Min % | Max % | # of Images |
| 21-Sep-2010 | 34.3% | 24.7% | 41.6% | 6 |
| 23-Sep-2010 | 34.0% | 28.2% | 38.3% | 13 |
| 4-Oct-2010 | 41.4% | 28.0% | 50.2% | 24 |
| 11-Oct-2010 | 31.5% | 19.0% | 47.7% | 28 |

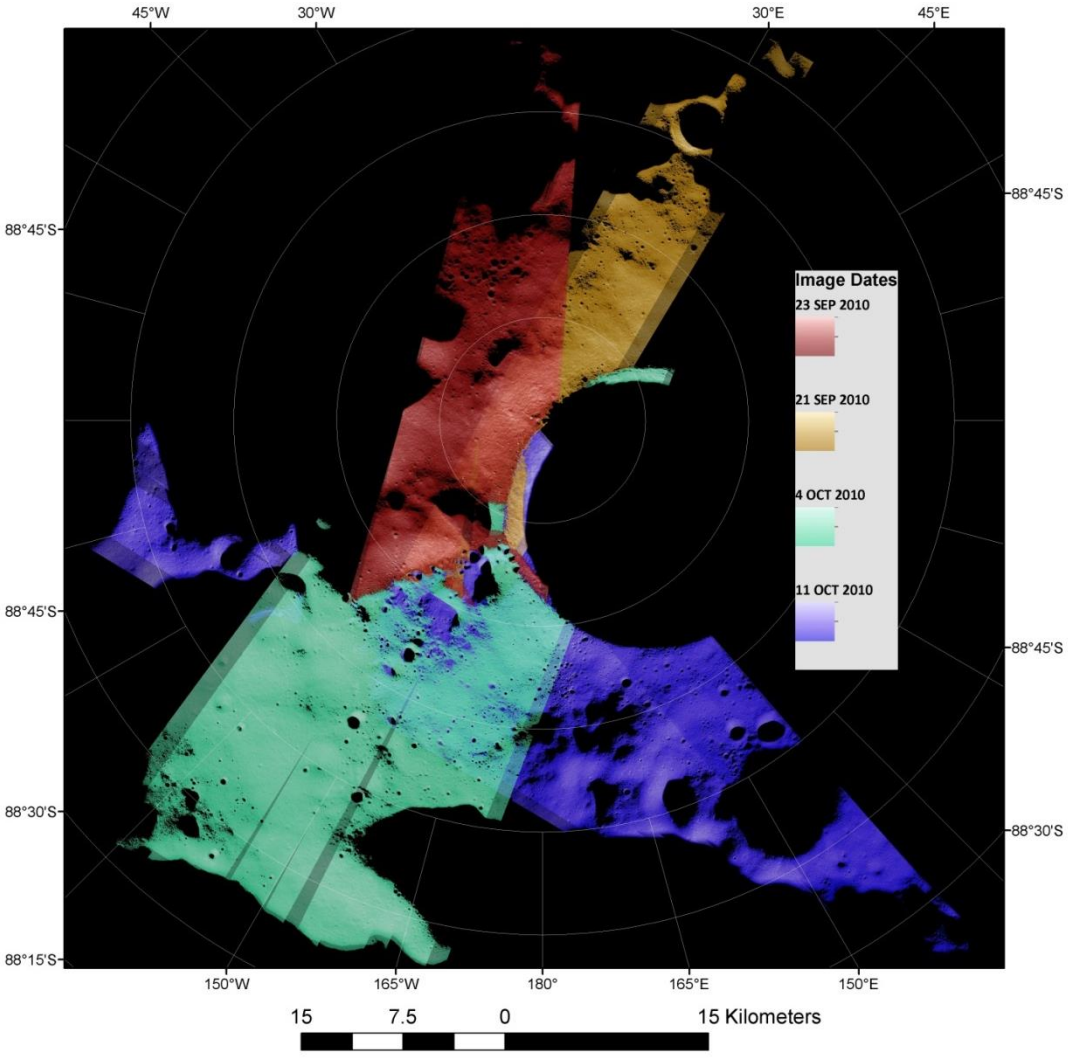


**Figure 1 - Area covered by LROC NAC images.**

### Expected Vertical Precision

Based on the spacecraft orbit and camera geometry, the theoretical expected vertical precision can be calculated. During the nominal mission, LRO is in a 50 km circular orbit. During image acquisition, LRO is either pointed nadir or rotated about the flight line (normal situation) to acquire a stereomate. In some cases, LRO can also be pitched forward to acquire stereo images in the polar regions. The convergence angle is the total parallax angle between the two stereo pairs. Based on the spacecraft geometry, we can calculate the expected vertical precision using base to height ratio, assuming the instantaneous field of view (IFOV) or ground sample distance (GSD) of 1 m, and feature match RMS error of 0.2 pixels (Cook and others, 1996). Figure 2 shows the expected vertical precision for convergence angle between 5 and 30 degrees for a 50 km orbit and images with a 1 m ground sample distance (GSD.) The images used in this work had a convergence angle of about 20° and they provide an expected precision of about 0.60 to 0.73 m, depending on the resolution of the image.

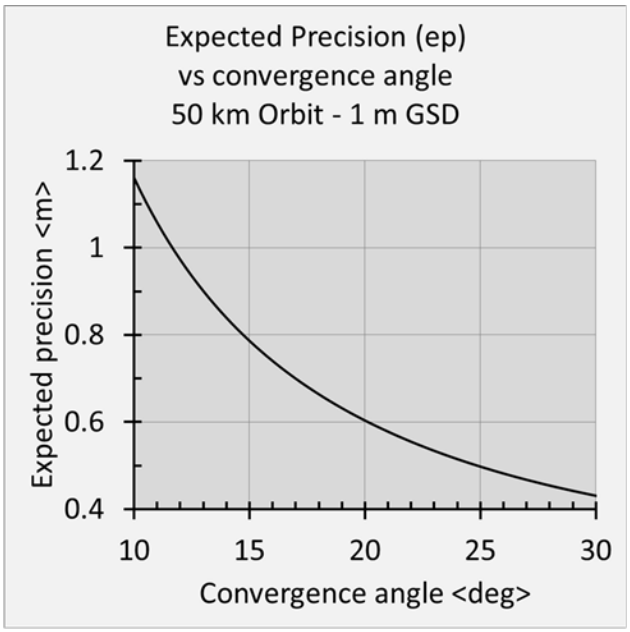


**Figure 2 - Expected precision**

### LOLA

LOLA is a pulse detection time-of-flight altimeter that incorporates a five-spot pattern to measure the precise distance to the lunar surface at 5 spots simultaneously, thus providing 5 profiles across the lunar surface for each orbit. LOLA fires at a fixed, 28-Hz rate, so that for a nominal 1600 m/s ground track speed there is one shot approximately every 57 m. The LOLA spot pattern is shown in Figure 3. At a nominal 50-km altitude, each spot within the five-spot pattern has a diameter of 5 m while each detector field of view has a diameter of 20 m. The spots are 25 meters apart, and form a cross pattern canted by 26 degrees counterclockwise to provide five adjacent profiles (PDS Geoscience Node, 2010; Smith and others, 2010; Zuber and others, 2010.) The LOLA instrument boresight is aligned with the LROC NAC cameras to enable altimetry data collection in the overlap region between the NAC_L and NAC_R.

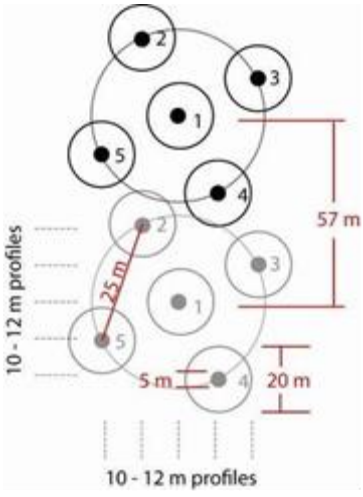


**Figure 3 - LOLA spot pattern**

Tracking of LRO is currently within 10 m radial and 300 m horizontal accuracy (Zuber and others, 2010). By using Earth-based laser ranging tracking and crossover analysis, the expected accuracy of the LOLA data

will be 1 m radial and 50 m horizontal.

### LOLA 5-m Grid

The LOLA team created a 5-m DEM of the lunar south pole that goes down to 87.5° S in a polar stereographic projection. The data are stored as integer values with a scale factor of 0.5 m relative to a radius of 1737.4 km; this results in the elevation values being binned into 0.5 m bins (i.e. 0.0, 0.5, 1.0, etc.) The version we used during this work was released March 2010. There was a new version released in March 2013 after we finished this work.

## Methodology

To generate the DEMs, we used a combination of the USGS Integrated Software for Imagers and Spectrometers (ISIS) (see http://isis.astrogeology.usgs.gov/) and SOCET SET. ISIS routines ingest the image files, perform a radiometric correction, and export to a format SOCET SET accepts. The NAC files imported into SOCET SET are Level 1 radiometrically corrected images and a list of keywords of relevant parameters, such as spacecraft coordinates, altitude, Euler angles, and ephemeris positions.

### Software modifications

SOCET SET's generic pushbroom sensor model failed when determining the time an image line was obtained for images that crossed the poles. We replaced its interpolation method with the more robust "Brent's Method," a root-finding algorithm (Brent, 1973.) Mapping with images acquired while the spacecraft was rotating was accomplished by supplying quaternions at an adequate interval that captures the rotation, to the sensor model. Quaternions describe the sensor pointing, and if not supplied, the sensor model will calculate default quaternions based on one instance of the sensor pointing, which is insufficient if the sensor pointing is not held reasonably constant. As a by-product, these quaternions also allow for a straight forward import of images into SOCET SET without the need to preprocess for boresight sample locations, image binning and mirrored (flipped) images.

### Bundle Adjustment

The spacecraft position and angles need to be adjusted so that the images are registered to each other and to the LOLA DEM. The images were grouped by the date they were collected and adjusted in those groups and then all four groups were adjusted together. In order to tie these groups together, extra image tie points were used around the rim and wall of Shackleton crater and along ridge lines where the images went into shadows.

Figure 4 shows the z-residual of the 1,008 z-control points used in the bundle adjustment. The z value is an estimate of the elevation value and is obtained from the LOLA 5-m DEM. As we iterate through the bundle adjustment we obtain better estimates for the horizontal location of the points and update the z estimate that we obtain from the LOLA DEM. The z-residual is the difference in the z value calculated by the final bundle adjustment and the estimate obtained from the LOLA DEM. Figure 5 shows the histogram of the z-residuals. The mean residual was -0.9 m with a standard deviation of 4.6 m. The residual ranged from -41.8 to 29.1 m.

Figure 6 shows the z-residual of the 106 xyz-control points used in the bundle adjustment. The xyz values of the control points are estimated by using the LOLA track points. When viewing the LOLA track points with the stereo images one can find morphological features that match. The xyz values of the LOLA track point are used as an estimate of the location of the morphological feature seen in the image. The xyz-residuals are the differences in the values calculated by the final bundle adjustment and the xyz values of the LOLA track point. Figures 7 – 9 show the histograms of the x, y, and z-residuals for the xyz control points. Figure 10 combines the x, y, and z residual into the total residual for the xyz control points. Table 2 provides the statistics for the xyz control point residuals. The horizontal errors (x and y residuals) are larger than the vertical error (z residual.) This is consistent with the LOLA data having a larger error in the horizontal direction than in the vertical direction. Figure 11 shows the total residual (xyz) for the xyz control points.

Table 2 - XYZ Control Points

| | Residual - m | | | | |
|---|---|---|---|---|---|
| | *X* | *Y* | *Z* | *XY* | *XYZ* |
| Mean | -5.4 | -1.0 | -0.6 | 15.0 | 15.5 |
| Median | -4.6 | -0.9 | -1.2 | 12.6 | 12.9 |
| Standard Deviation | 13.9 | 10.2 | 3.4 | 10.0 | 9.8 |
| Range | 76.1 | 55.1 | 16.2 | 47.4 | 47.0 |
| Minimum | -40.2 | -29.8 | -7.8 | 0.9 | 1.6 |
| Maximum | 35.9 | 25.3 | 8.4 | 48.3 | 48.5 |

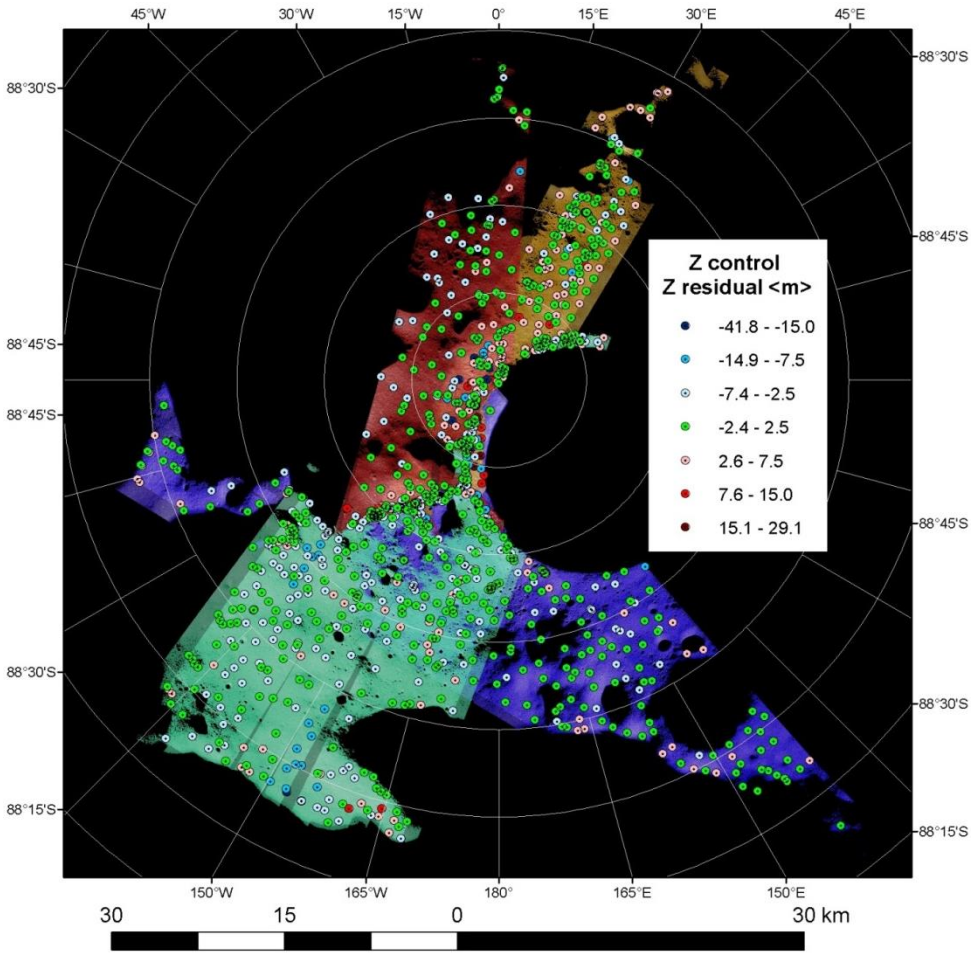


**Figure 4 - Z-residual component of the Z control points.**

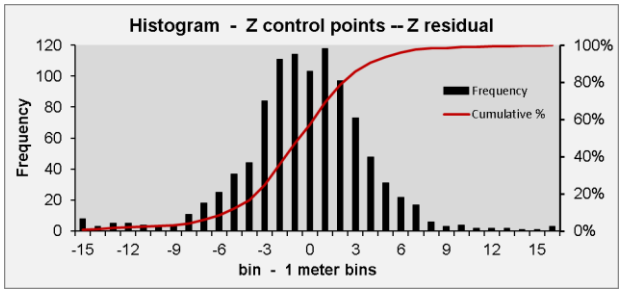


**Figure 5 - Histogram of z-residuals for the z-control points.**

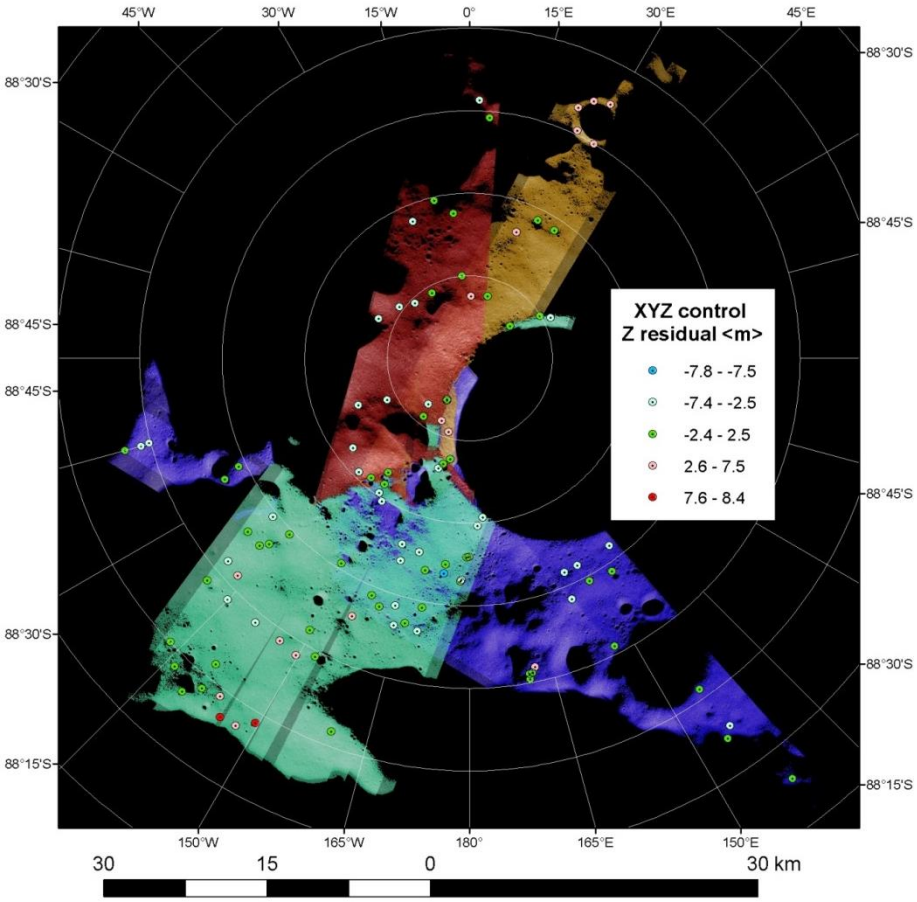


**Figure 6 - Z-residual component of the XYZ control points.**

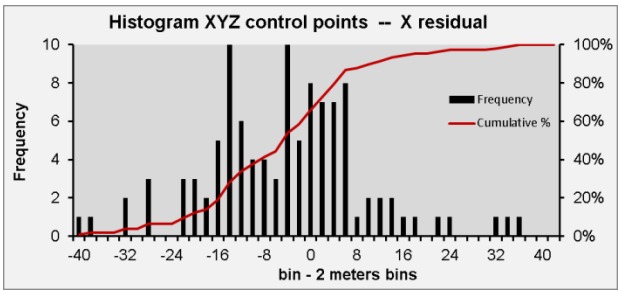


**Figure 7 - Histogram of x-residuals.**

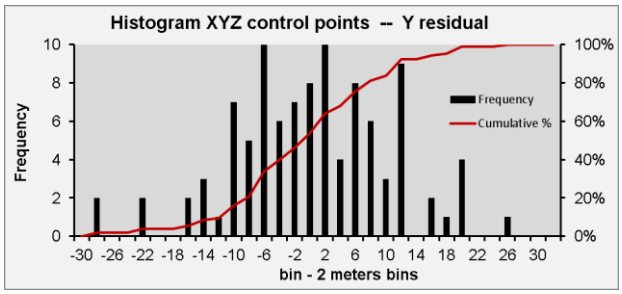


**Figure 8 - Histogram of y-residuals.**

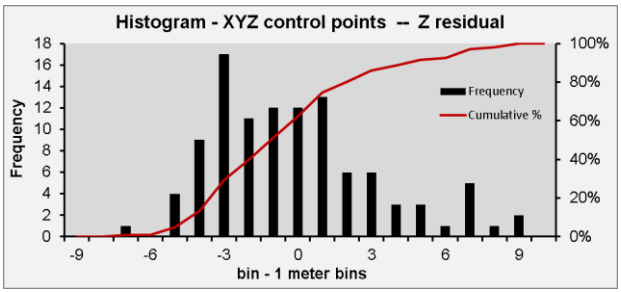


**Figure 9 - Histogram of z-residuals.**

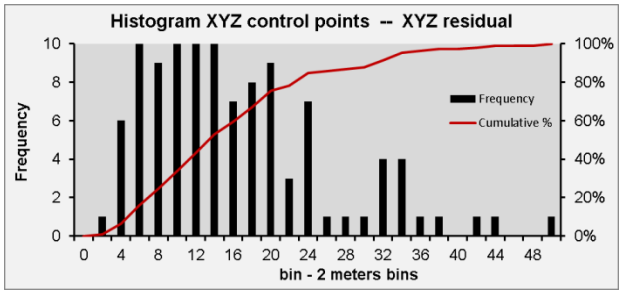


**Figure 10 - Histogram of xyz-residuals.**

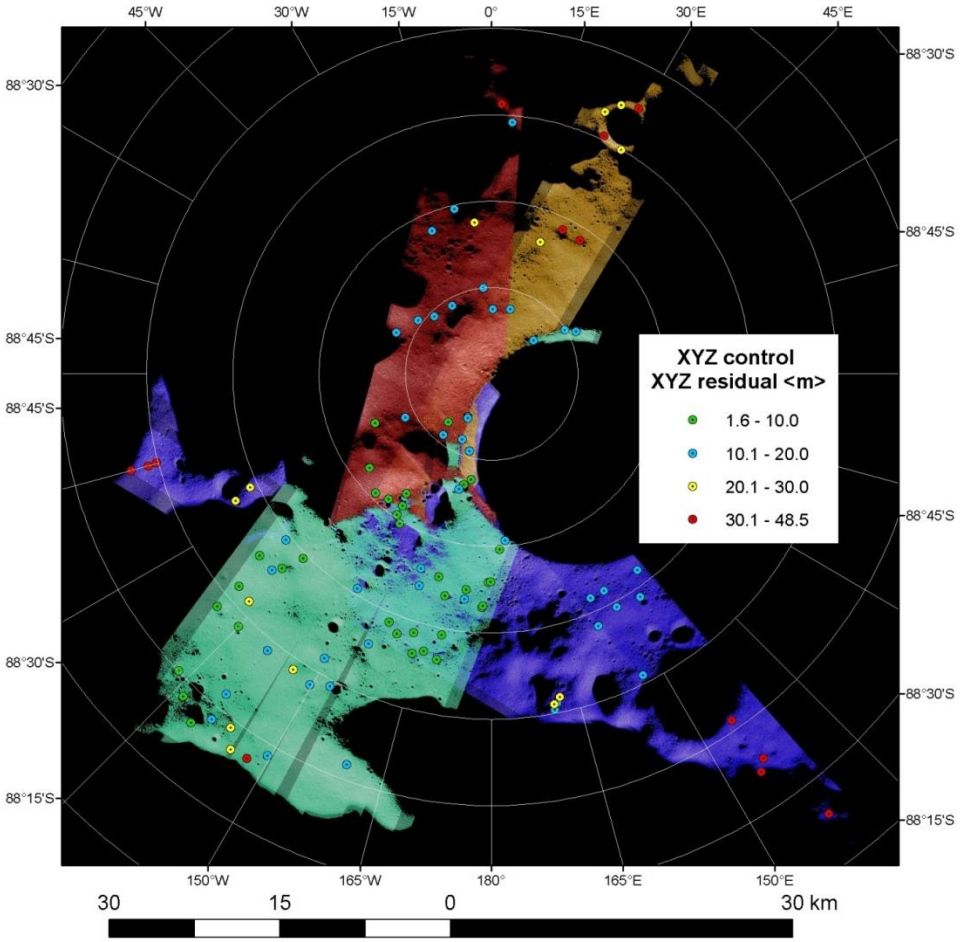


**Figure 11 - XYZ residual component of XYZ control point.**

## DEM Extraction

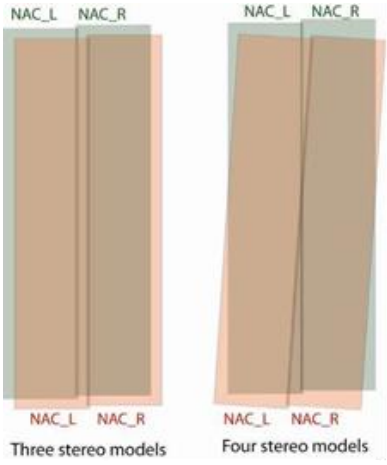


**Figure 12 - Stereomodels**

After the images are adjusted, DEMs can be extracted from the stereomodels. For this project we used 67 images and collected 76 DEMs that were merged into a final DEM. The DEM extraction software is not optimized to work with linear pushbroom images (Zhang and others, 2006.) One way to increase the effectiveness is to perform a pair-wise rectification on the images that will be used in the DEM extraction. This process rotates the images so that the epipolar lines are horizontal and scales the images to a common pixel scale. The rectified images reduces the eye strain of looking at stereo images and are required for accurate generation of the DEM. Another way to increase the effectiveness is to generate a continuous rational polynomial sensor model for the images. The advantage of this method is that if pair-wise rectification is used, then 3 or 4 sets of

images would need to be generated (NAC_L – NAC_L, NAC_R – NAC_R, NAC_L – NAC_R, NAC_R – NAC_L) depending on how many stereo models are formed by the LROC NAC images (Figure 12.) The continuous rational polynomial sensor model images can be combined with different images since they are generated independent of any other image.

## Output Products

Our standard products include the DEM, color shaded relief image (Figure 13,) and slope map (Figure 23) provided in GeoTIFF format. The LOLA 5-m DEM is shown as a color shaded relief image in Figure 14 and as slope map in Figure 24 for comparison. Figures 15 and 16 provide a close-up of the color shaded relief images for the LROC NAC and LOLA DEM.

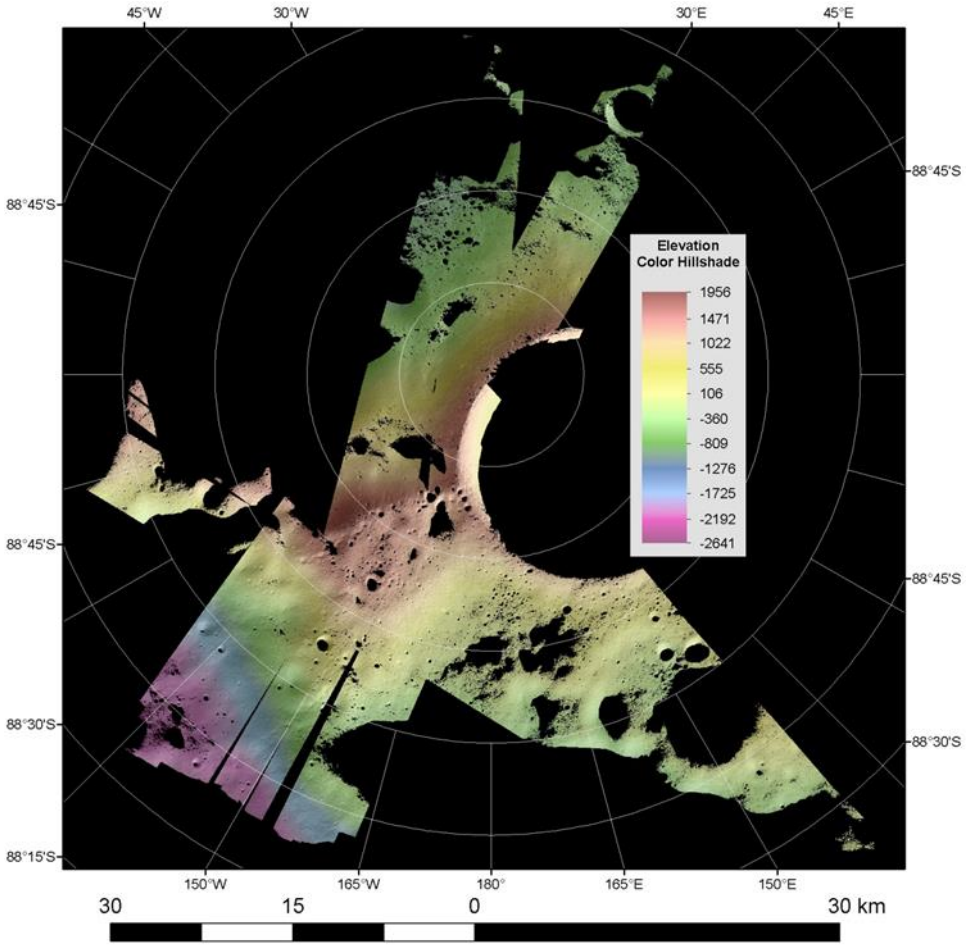


**Figure 13 - LROC NAC color shaded relief image.**

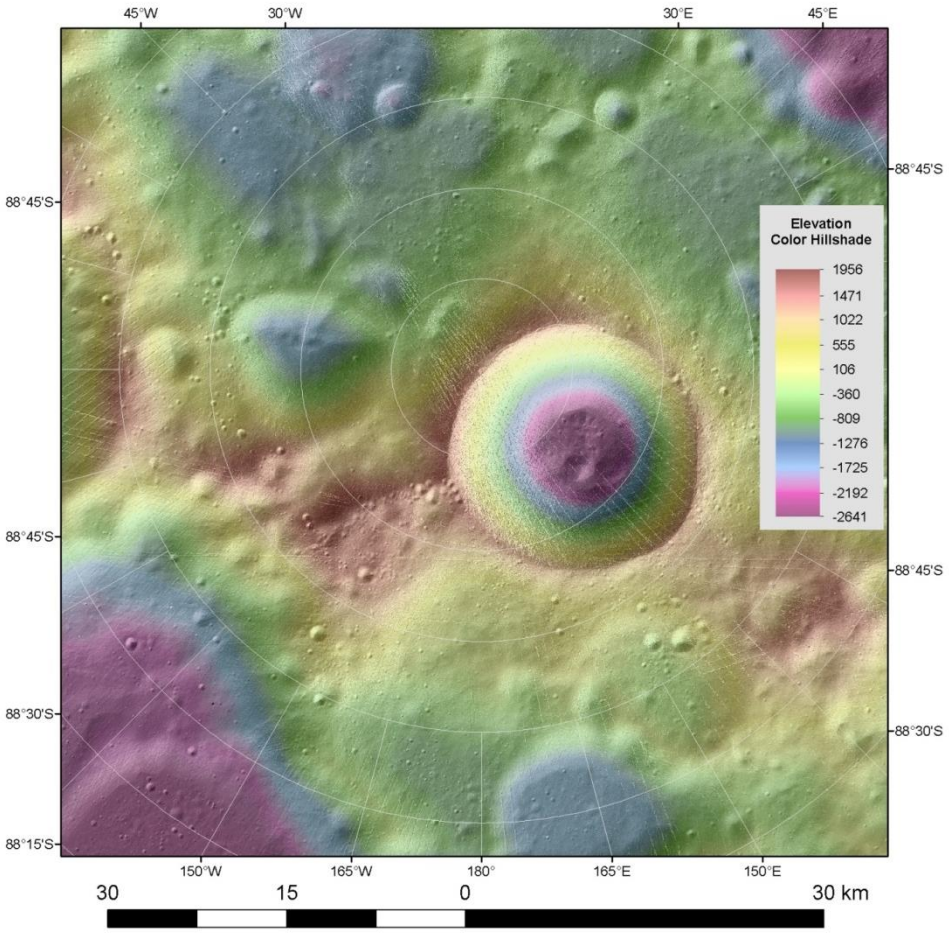


**Figure 14 - LOLA DEM color shaded relief image.**

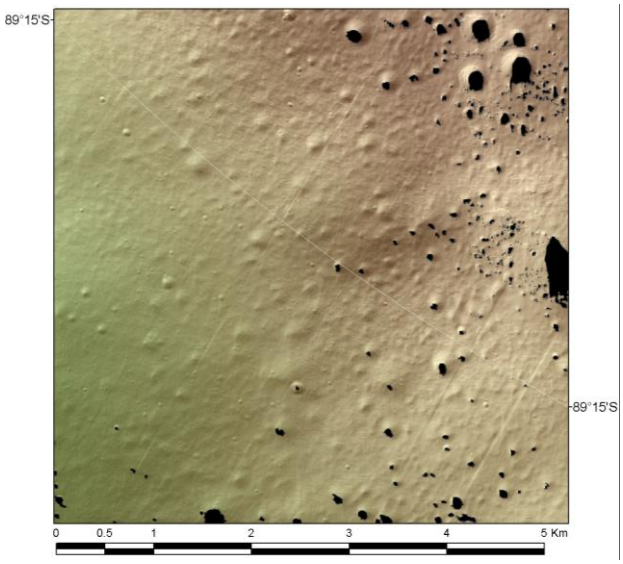


**Figure 15 - Close-up of LROC NAC DEM color shaded relief image.**

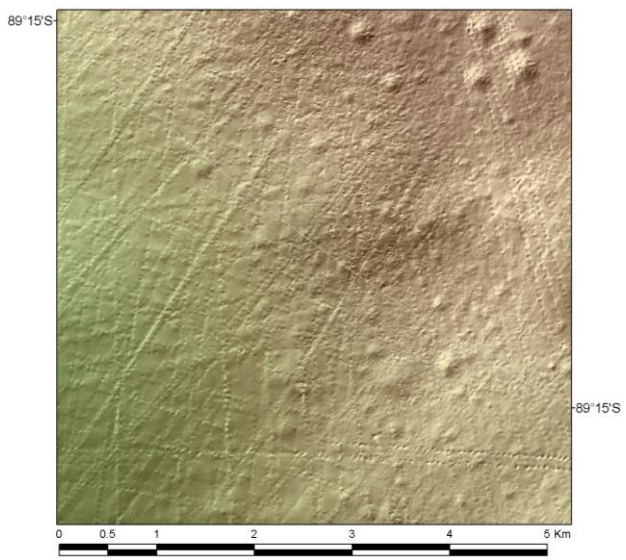


**Figure 16 - Close-up of LOLA DEM color shaded relief image.**

## Error Analysis

### Elevation values

The elevation value differences between the LROC NAC DEM and the LOLA DEM are presented in Figure 17. There are 20,349 points that have a difference larger than ±50 m (0.0306%) and 234,793 points that have a difference of larger than ±25 m ( 0.3528%.) If we remove these outliers, then the mean difference is -0.9 m with a standard deviation of 4.8 m and -0.8 with a standard deviation of 4.4 m, respectively. These outliers are most likely caused by horizontal offsets in the LOLA tracks. The other main source that causes the differences is from not properly modeling the motion of the spacecraft.

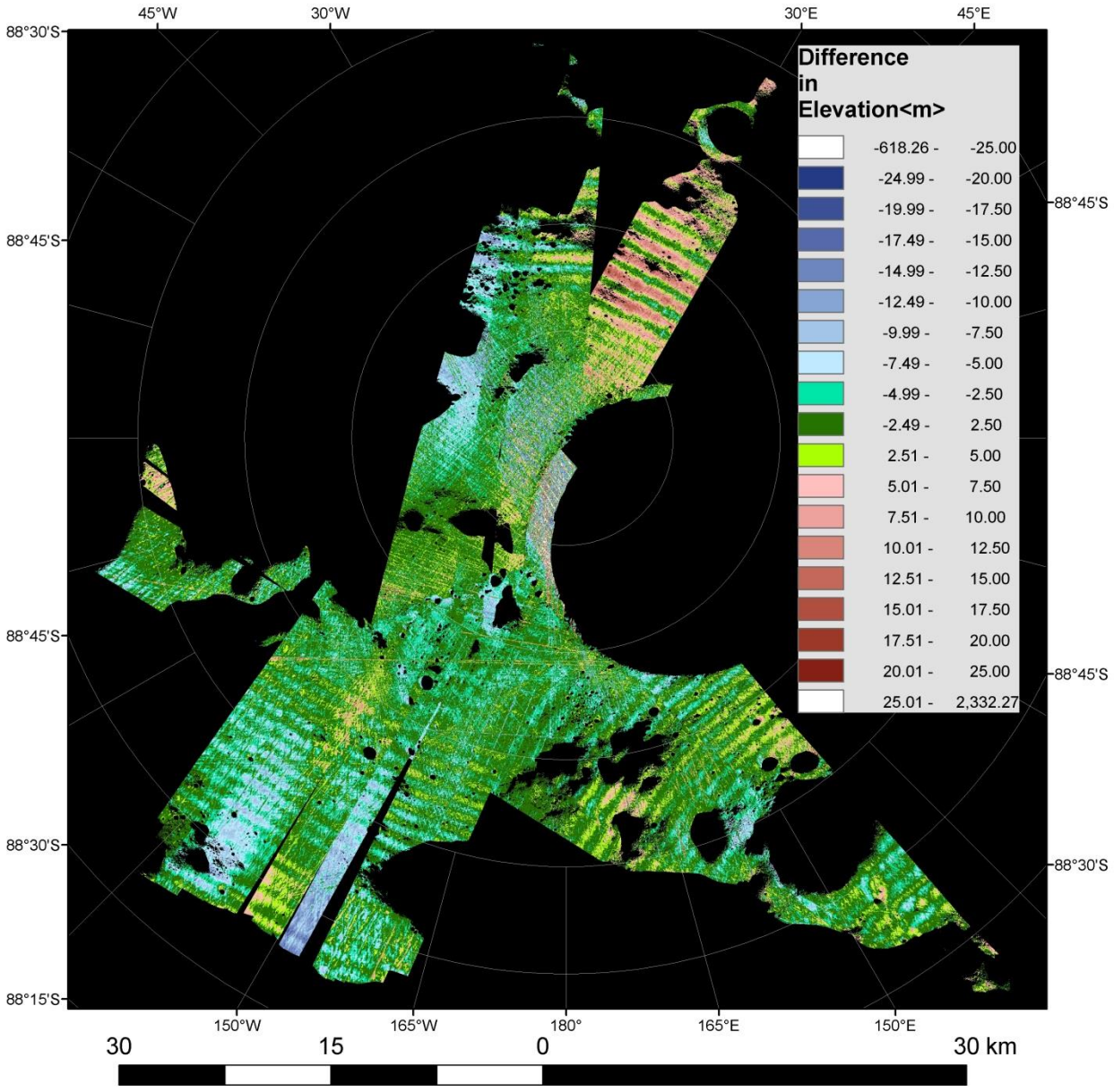


**Figure 17 -- Elevation value differences between LROC NAC and LOLA DEM.**

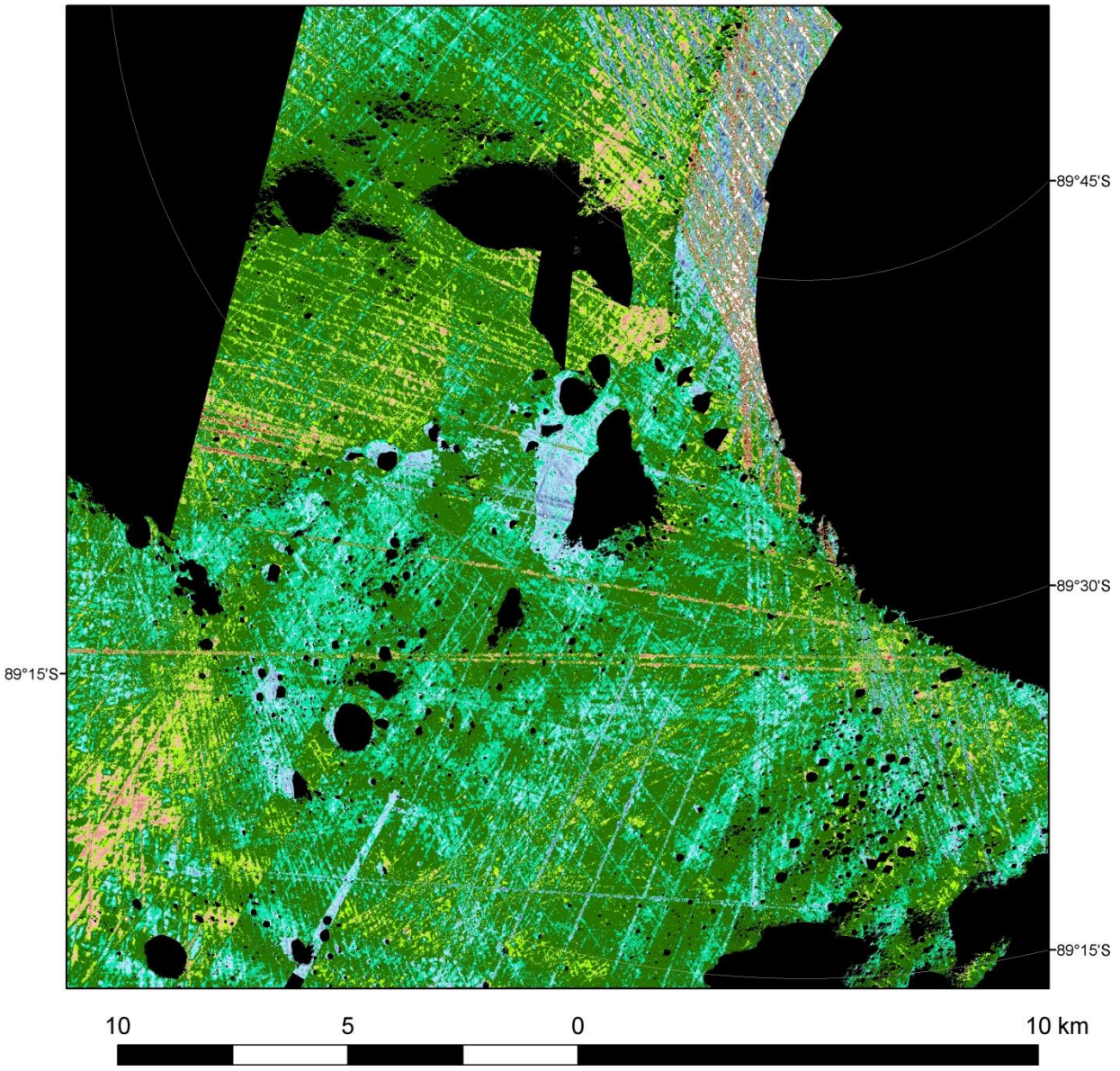


**Figure 18-- Elevation differences dominated by horizontal offsets in the LOLA data.**

In Figure 18 we are focused on the area where the four sets of images come together, which is by the rim of Shackleton crater. The differences are predominated by linear features. These features are LOLA tracks that probably have a horizontal offset. The differences are greatest along the wall of Shackleton crater where the slopes are larger and any horizontal offset would cause a larger difference.

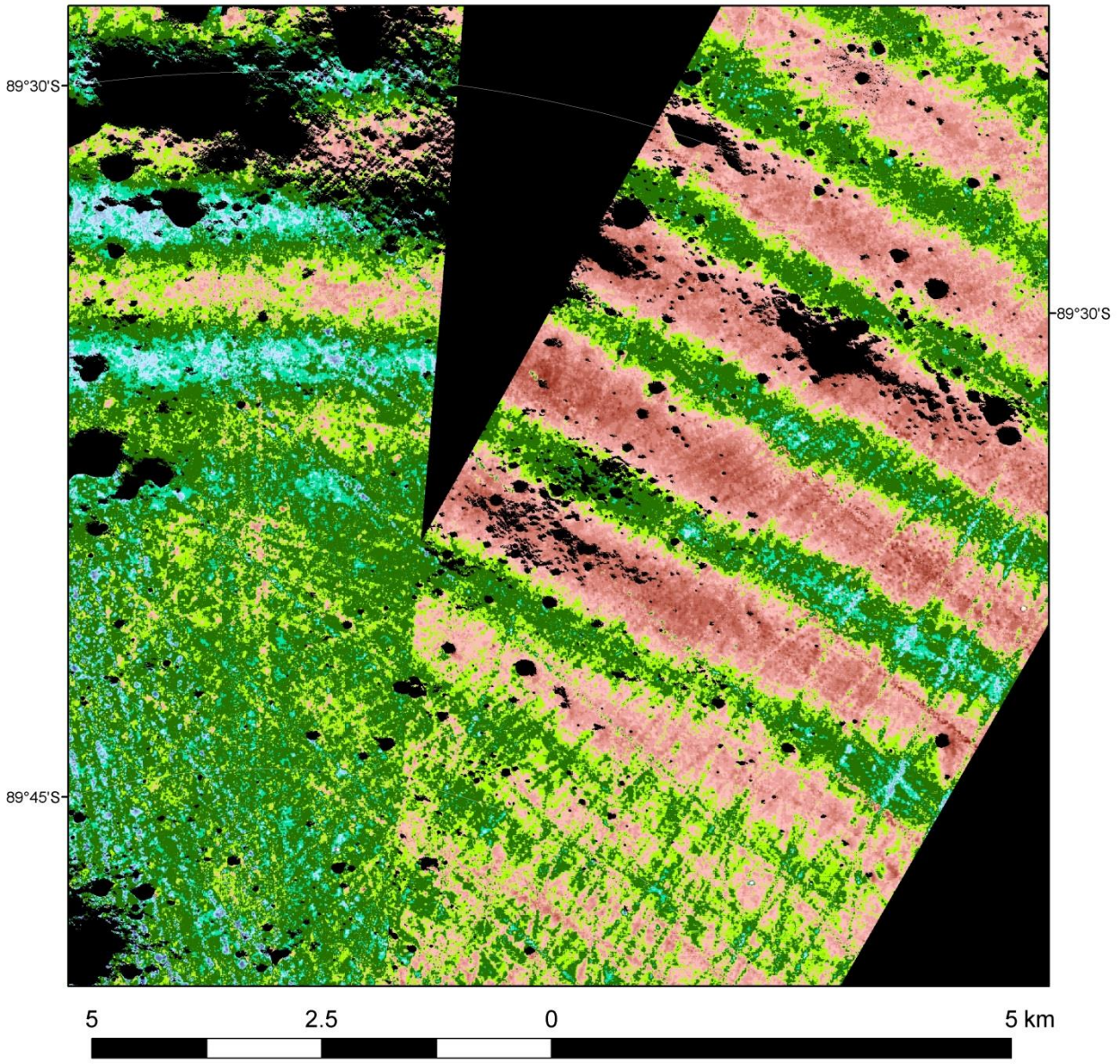


**Figure 19 Elevation differences dominated by spacecraft motion that is not modeled.**

In Figure 19 the differences are mainly caused by spacecraft motion that is not modeled properly by the sensor model. On the right hand side of the image are stereomodels from 21 SEP 2010 and on the left hand side are stereomodels from 23 SEP 2010. The alternating red and green bands on the right hand side of the image show differences in the range of -6 to 15 m. In Figure 20 the offset from the average spacecraft angles omega and phi for image M139716114LE are plotted along with differences in elevation values between the LROC NAC and LOLA DEM. Between the time -12 to -9 seconds, the amplitude of omega and phi are varying from -.002° and +.00025° and the elevation differences range from -0.5 to 15 m. The spacecraft is more stable between the time -7 to -5 seconds and the range of elevation differences is lower and between -6 and +6 m.

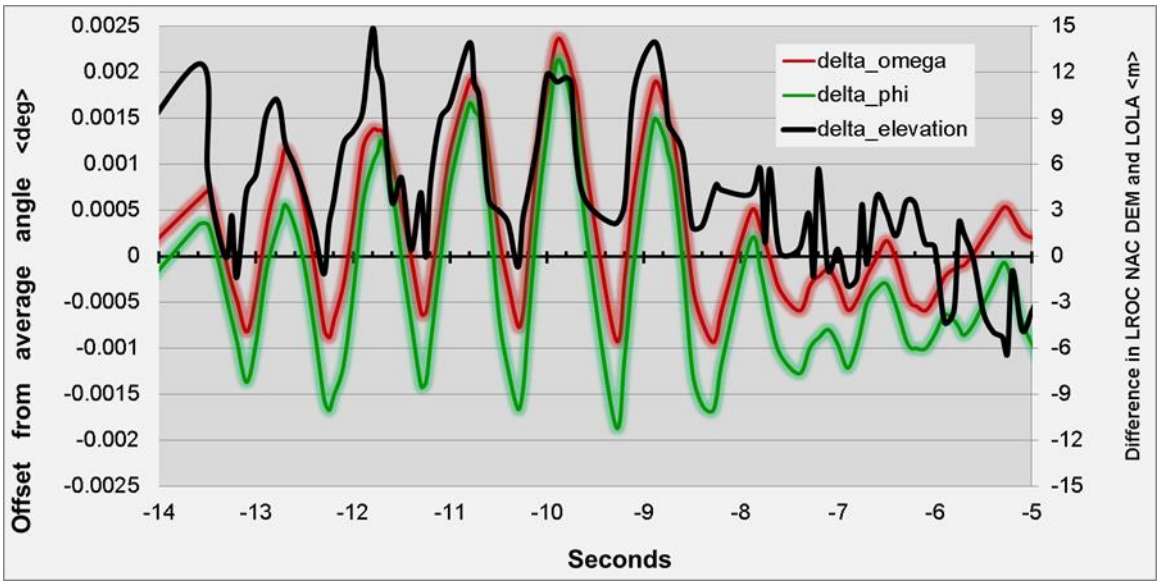


**Figure 20 - Chart of spacecraft motion and elevation differences.**

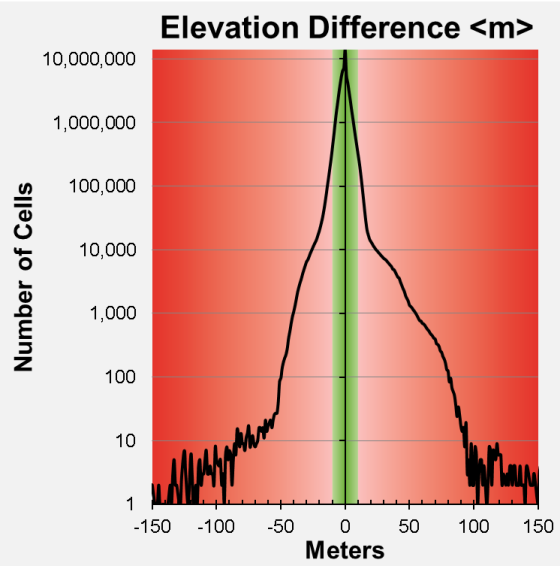


| Difference in Elevation | |
|---|---|
| Meter | Per Cent |
| ±0 | 21% |
| ±1 | 40% |
| ±2 | 56% |
| ±3 | 69% |
| ±4 | 78% |
| ±5 | 84% |
| ±6 | 89% |
| ±7 | 92% |
| ±8 | 94% |
| ±9 | 96% |
| ±10 | 97% |

**Figure 21 - Histogram of elevation differences.**

The elevation differences are mainly between ±10 m; with 56% of the elevation differences within the expected precision of ±2 m.

## Slope values

Slight differences are to be expected between the slope values calculated from the LROC NAC and LOLA DEM due to the differences in the post spacing for the DEMs. The LROC NAC DEM has a 4 m post spacing so the baselines in the slope calculation are 8 m (horizontal and vertical cells) and 11.3 m (diagonal cells)


**Figure 22 - Legend for slope maps.**

The LOLA 5-m DEM has 5 m post spacing so the baselines in the slope calculation are 10 m (horizontal and vertical cells) and 14.1 m (diagonal cells) The slope maps were created with the same color look-up table that stretched slope values between 0° and 30° in shades of green, between 31° and 45° in shades of yellow to brown, and between 46° and 90° in shades of red. Slopes in the first group are values that are to be expected, slopes in the middle group occur mainly along crater walls, and slopes in the third group are unusual and might be erroneous. In editing the LROC NAC DEM we looked for large areas where the slopes were above 45° to edit. There are 3,176 cells (0.0048%) in the LROC NAC DEM with slopes above 45°. Within the LOLA DEM there are 799,651 cells (1.2015%) with slope values above 45°. The LROC NAC DEM improves upon the slope values within the LOLA DEM.

In Figure 23 the slope values for the LROC NAC DEM are presented. Along the wall of Shackleton crater there are some slope values above 45°. During editing we tried to smooth this area and without completely re-doing this area by hand we had to leave some of these data in the DEM. The color look up table for all slope maps is shown in Figure 22.

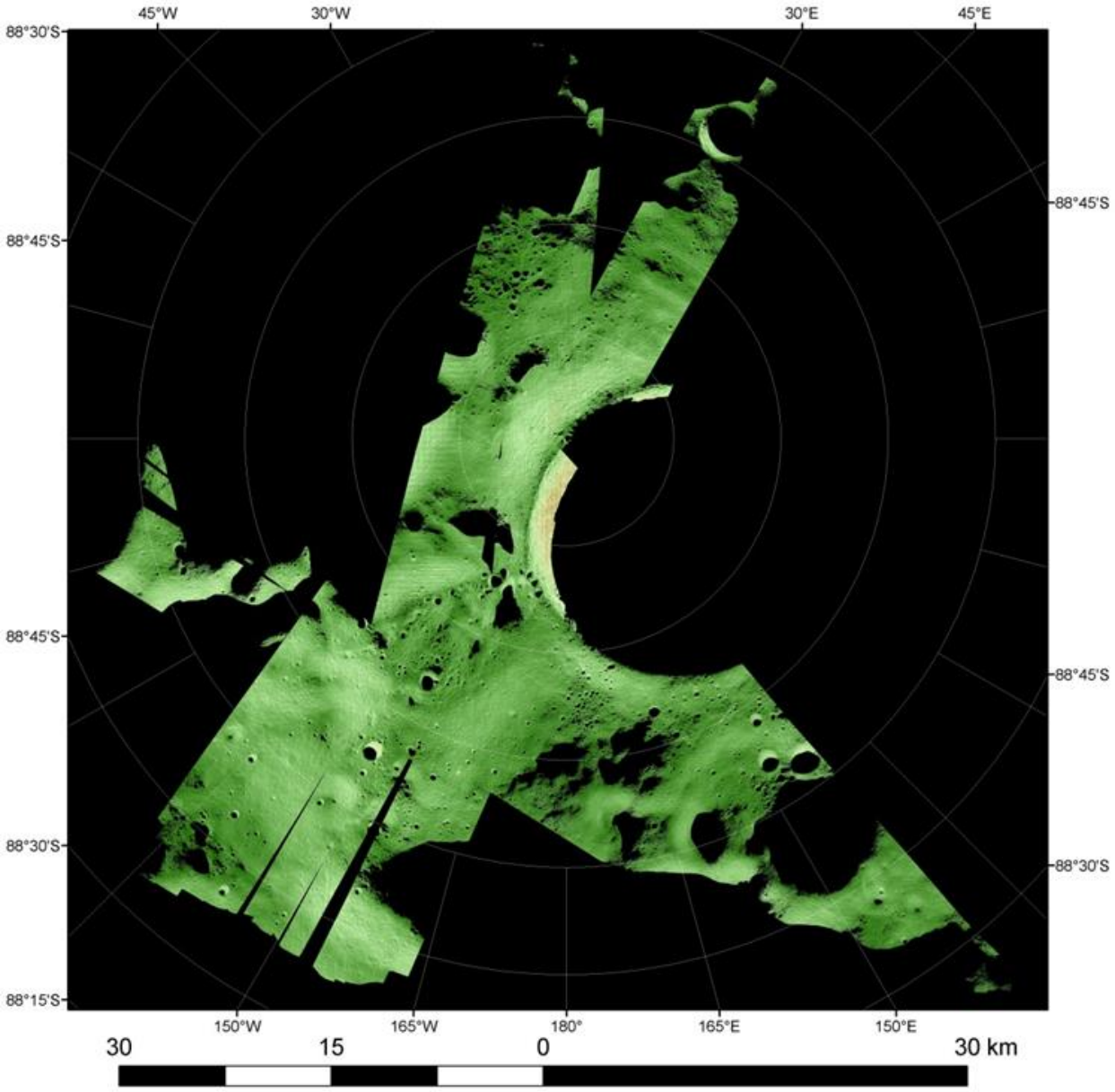


**Figure 23 - LROC NAC Slope Map.**

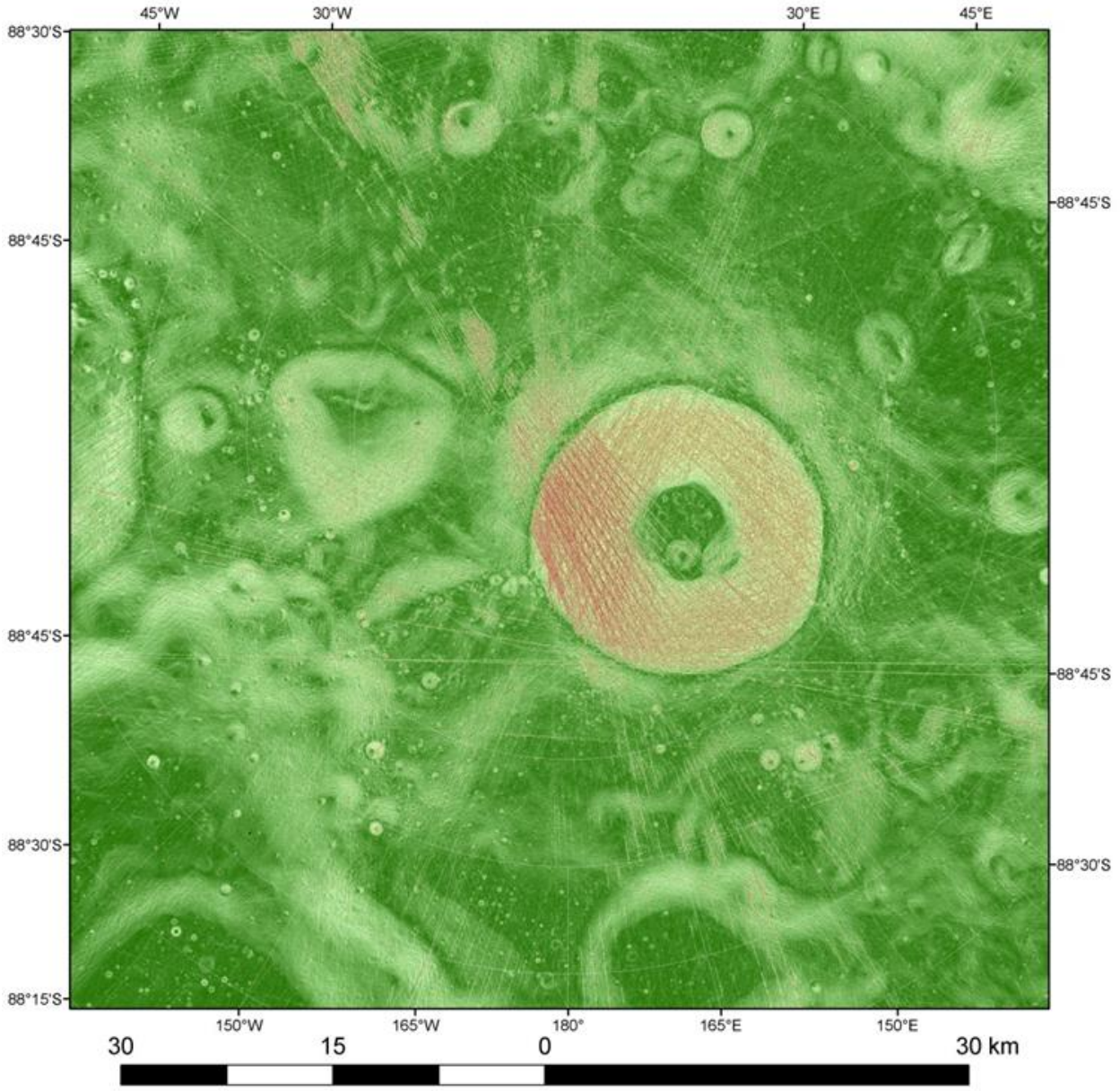


**Figure 24 - LOLA 5-m GRID Slope map.**

In Figure 24 the slope map for the LOLA 5-m DEM is presented. The LOLA DEM is released with the elevation values rounded to the nearest 0.5 m. This causes the slope values to be non-continuous and there are steps between slope values as large as 2°. In Figure 25 the differences between LOLA and LROC NAC slope values are presented. There are some areas where the un-modeled spacecraft motion affects the slope values and in other areas the horizontal offset in the LOLA tracks affect the differences in the slope values. In Figure 26 histograms of the slope values are presented. The count distribution histogram shows the non-continuous nature of the LOLA slope values and the Cumulative distribution shows that almost all of the slopes in the LROC NAC DEM are below 30°.

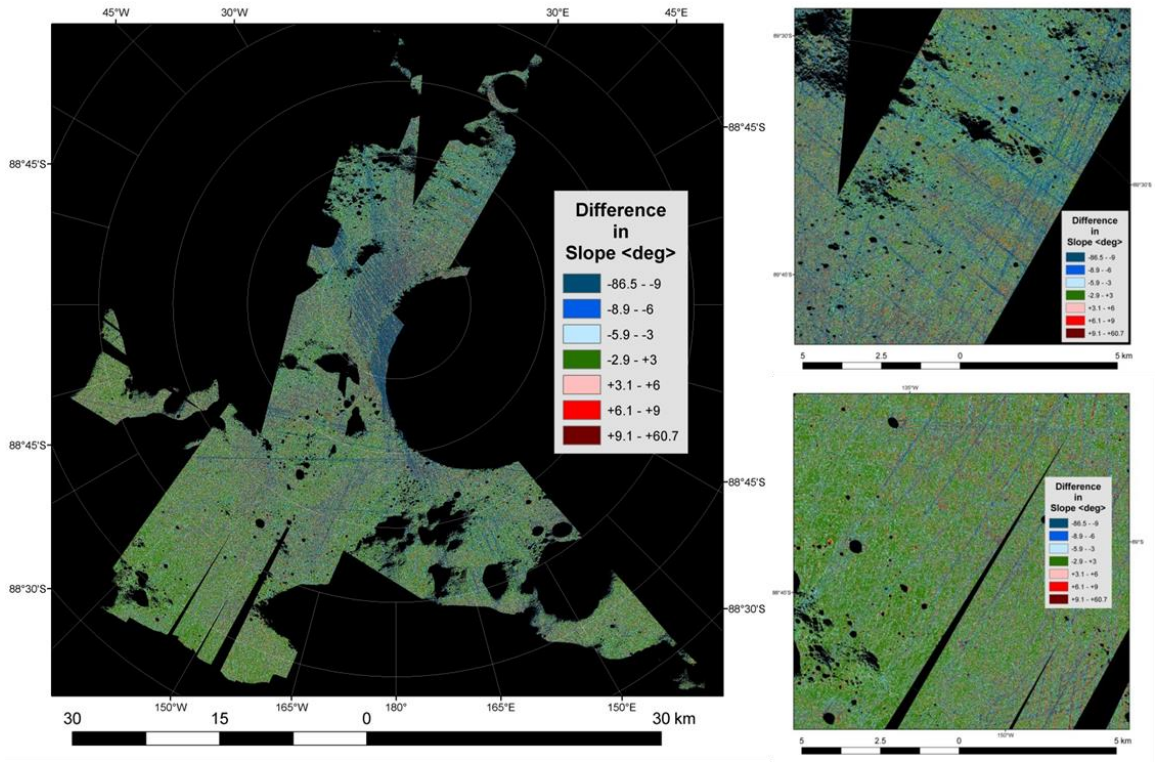


**Figure 25 - Map of the differences in slope values between LROC NAC and LOLA.**

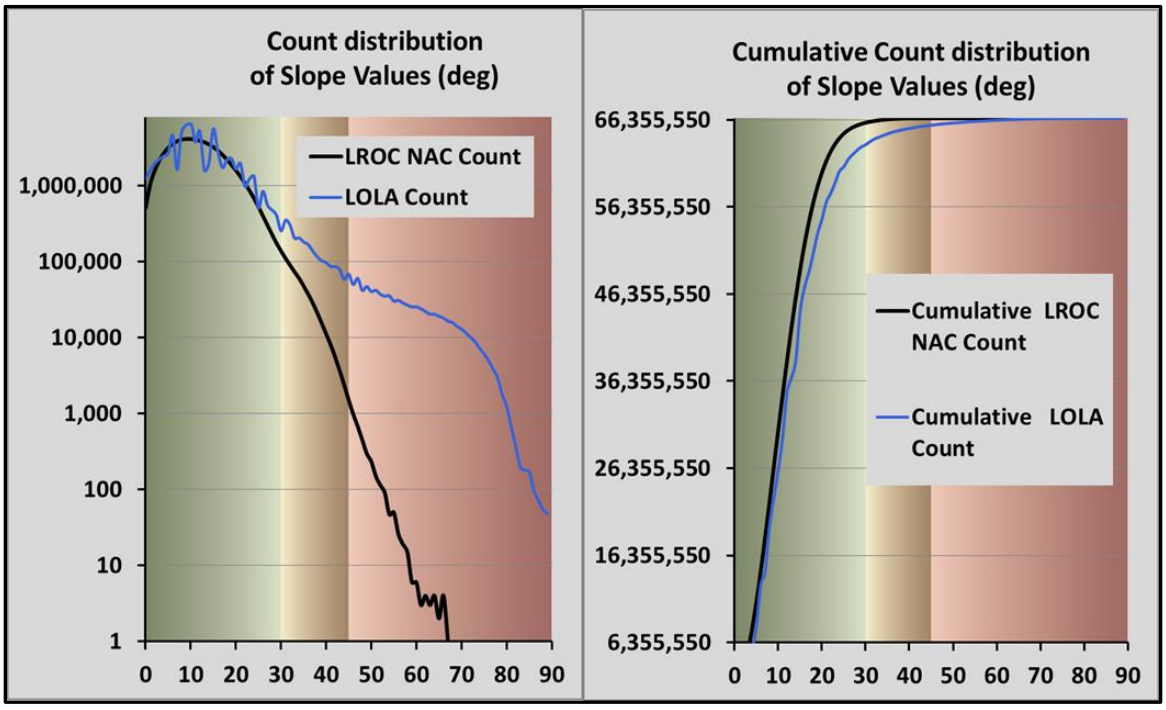


**Figure 26 - Histograms of differences in slope values for LROC NAC and LOLA.**

## Conclusions

The LROC NAC 4-m DEM can be used for analysis of slopes in the south pole lunar region. There are seams of 1 – 5 m between the stereomodels that will need to be avoided. These can easily be found as they will appear as linear features in the slope map. There are errors near the shadows in the images that might contain erroneous data. Due to un-modeled image motion there can be areas with systematic errors of 5 – 15 m (Figures 17 - 20.) For applications of siting of communication towers or solar arrays on towers that require measurements over large distances, this could cause a problem. For slope analysis this would be less of a problem because in a local area the errors are less.

A way to improve the modeling of the image motion in line scanner imaging systems (i.e. pushbroom sensors) would be to improve the registration of the LOLA track data to the images, be able to adjust the position of the LOLA track data, and to combine this with information from overlapping stereomodels to improve how the sensor angles (omega, phi, and kappa) are computed for the lines within the line scanner images. This would be possible within the ISIS software program *jigsaw* with slight adjustments to the parameters.. Within the *jigsaw* program, we can model the image motion with an $n^{th}$ order polynomial and we could add constraints that use the range information from the LOLA track data and elevation information from overlapping stereomodels to provide constraints that would ensure any adjustment to the image motion would be reasonable. This would result in reducing the seams between stereomodels and providing adjusted LOLA track data with improved information about the horizontal position of the LOLA track points.

## References


Brent, R.P.; (1973) Algorithms for Minimization without Derivatives, Chapter 4. Prentice-Hall, Englewood Cliffs, NJ.

Cook, A.C. ; Oberst, J.; Roatsch, T.; Jaumann, R.; Acton, C.; (1996) Clementine imagery: selenographic coverage for cartographic and scientific use, Planetary and Space Science Volume 44, Issue 10, October 1996, Pages 1135–1148.

de Venecia, Kurt J.; Racine, R.; and Walker, A. S.; (2005) End-To-End Photogrametry for Non-Professional Photogrammetrists, ASPRS 2005 Annual Conference, Geospatial Goes Global: From Your Neighborhood to the Whole Planet, March 7-11, 2005, Baltimore, Maryland.

Nall, M.; French, R.; Noble, S.; Muery, K.; and the LMMP Team; (2010) The Lunar Mapping and Modeling Project, Annual Meeting of the Lunar Exploration Analysis Group, held September 14-16, 2010 in Washington, DC. LPI Contribution No. 1595, p.47.

Neumann G. A.; (2010) Lunar Orbiter Laser Altimeter Raw Data Set, LRO-L-LOLA-4-GDR-V1.0, NASA Planetary Data System.

Noble, S. K.; French, R. A.; Nall, M. E.; Muery, K. G.; (2009) The Lunar Mapping and Modeling Project, Annual Meeting of the Lunar Exploration Analysis Group, held November 16-19, 2009 in Houston, Texas. LPI Contribution No. 1515, p.48

PDS Geoscience Node, (2010, checked 3 April 2013), http://pds-geosciences.wustl.edu/ , http://imbrium.mit.edu/LOLA.html , and http://ode.rsl.wustl.edu/moon/ .

Rosiek, M. R.; Lee, E. M.; Howington-Kraus, E. T.; Fergason, R. L.; Weller, L. A.; Galuszka, D. M.; Redding, B. L.; Thomas, O. H.; Saleh, R. A.; Richie, J. O.; Shinaman, J. R.; Archinal, B. A.; Hare, T. M.; (2012) USGS Digital Terrain Models and Mosaics for LMMP,43rd Lunar and Planetary Science Conference, held March 19–23, 2012 at The Woodlands, Texas. LPI Contribution No. 1659, id.2343.

Rosiek, M. R.; Thomas, O.; Howington-Kraus, E.; Foster, E.; (2013) Lunar South Pole Digital Elevation Models from Lunar Reconnaissance Orbiter Narrow Angle Camera, 44th Lunar and Planetary Science Conference, held March 18-22, 2013 in The Woodlands, Texas. LPI Contribution No. 1719, p.2583.

Tran, T.; Rosiek, M.R.; Beyer, R. A. ; Mattson, S.; Howington-Kraus, E.; Robinson, M.S.; Archinal, B.A.; Edmundson, K.; Harbour, D.; Anderson, E.; and the LROC Science Team; (2010) ISPRS Technical Commission IV & AutoCarto in conjunction with ASPRS/CaGIS 2010 Fall Specialty Conference November 15-19, 2010 Orlando, Florida, http://www.isprs.org/proceedings/XXXVIII/part4/files/Tran.pdf - checked 3 APR 2013.

Zhang, B.; Miller, S.; DeVenecia, K.; and Walker, S.; (2006) Automatic terrain extraction using multiple image pair and back matching. ASPRS 2006 Annual Conference, Reno, Nevada, 1 – 5 May. Unpaginated CD-ROM, 12 pp.